Carbon molecular sieve membranes derived from crosslinkable polyimides for CO_2/CH_4 and C_2H_4/C_2H_6 separations

Qixiang Wang[a] Fei Huang[bc] Chris J.Cornelius[b] & Yanfang Fan[a]

Abstract

Carbon molecular sieve (CMS) membranes were fabricated using carboxylated polyimides with various 6FpDA:DABA molar ratios. The as-prepared 6FDA-6FpDA:DABA multiblock polyimide, thermally crosslinked ones, and CMS membranes were characterized for CO_2/CH_4 and C_2H_4/C_2H_6 separation performance. Thermally crosslinked polyimide membranes due to decarboxylation exhibited increased gas permeability over uncrosslinked ones. All CMS membranes had enhanced gas separation performance as compared to their unmodified precursor polymer. A representative CMS membranes pyrolyzed at 576 °C had CO_2 and C_2H_4 permeability of 3573 and 244.6 Barrer with a CO_2/CH_4 and C_2H_4/C_2H_6 ideal selectivity of 51.5 and 4.80. A CMS membrane pyrolyzed at 800 °C had a C_2H_4 permeability of 10.4 Barrer and a C_2H_4/C_2H_6 ideal gas selectivity of 24.1. Increasing polyimide pyrolysis temperature improved CMS membrane gas selectivity but reduced its permeability. Zn^{2+} functionalized CMS membranes exhibited enhanced gas selectivity with a slight permeability reduction. The CMS membranes excellent gas separation performances surpassed Robeson's upper-bound. These materials hold great potential for industrial applications such as CO_2 separation and olefin recovery.

Graphical abstract
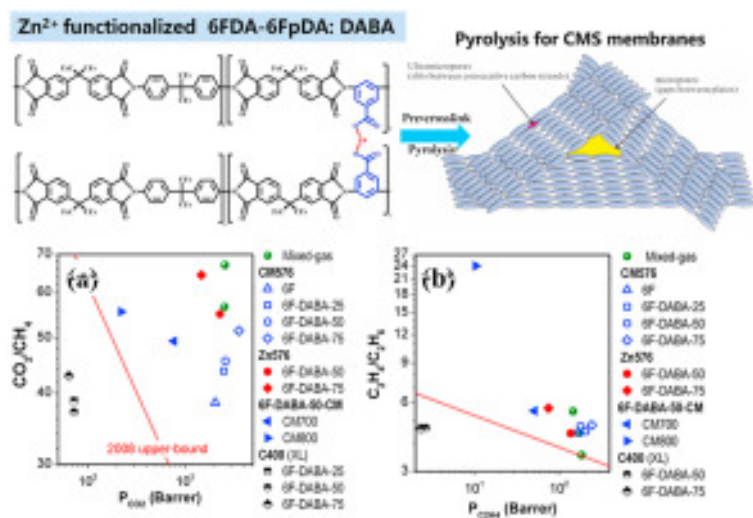
Keywords

1. Introduction

Membrane technology has gained extensive interest from researchers due to its energy-efficiency possibilities [1,2]. It holds significant potential for replacing conventional separation approaches such as cryogenic distillation and chemical absorption [3,4]. Today, membrane-based gas separations have been investigated for separating H_2/CO_2, H_2/CH_4, and CO_2/CH_4 [[5], [6], [7]], which extends to olefin/paraffin separations with modest size variations [8,9]. Polymer-based membranes are relatively competitive gas separation materials, but they suffer from a trade-off relationship between gas permeability and selectivity, characterized by Robeson's upper-bound [10,11]. Carbon molecular sieve (CMS) membranes derived from polymer precursors are excellent platforms to develop advanced membranes that may surpass this upper-bound.

CMS membranes are one type of molecular sieving material with a narrow pore size distribution. Their angstrom level channels can efficiently discriminate gases with subtle size variations [2]. Koresh et al. [12] prepared various hollow fiber CMS membranes using phenolic resin, polydecyl alcohol, polyacrylonitrile, and polyimide as organic precursors due to excellent thermal stability and mechanical behavior. In particular, CMS membranes derived from polyimides using 4,4′-hexafluoroisopropylidene diphthalic anhydride (6FDA) were extensively investigated for CO_2 and ethylene separations [[13], [14], [15], [16], [17]]. In a recent study, Qiu and Koros et al. [18] prepared a CMS membrane using 6FDA-mPDA:DABA (3:2) pyrolyzed at 550 °C. The CMS membranes had a CO_2 permeability reaching 14,750 Barrer with a CO_2/CH_4 selectivity of approximately 52. Fu et al. [13,19] generated CMS membranes from polyimides synthesized using 6FDA, diethyl toluene diamine (DETDA), and 3,5-diamino benzoic acid (DABA) to create 6FDA/DETDA:DABA (3:2) and 6FDA/DETDA. The 6FDA/DETDA:DABA (3:2) based CMS membrane had a CO_2 permeability of 21,740 Barrer that is almost eight times greater than a CMS material derived from 6FDA/DETDA. Karunaweera et al. [20] pyrolyzed 6FDA-DABA yielding a CMS membrane with C_3H_6 permeability of 400 Barrer and C_3H_6/C_3H_8 selectivity as high as 25. These various studies suggest that 6FDA-based polymers are desirable CMS membrane precursor candidates. Various co-polyimide chemical structures are designed using numerous dianhydride and diamine combinations. The polyimide –COOH functionality and concentration are essential variables used to positively affect a CMS membrane's properties.

CMS membranes are commonly created by pyrolyzing a polymer film at temperatures beyond 500 °C within an inert atmosphere or a vacuum. Their gas separation properties are intimately correlated with the pyrolysis procedure. The final pyrolysis temperature, atmosphere, soaking time, heating rate, and post-processing steps are critical parameters dictating a CMS membrane's properties [[21], [22], [23], [24], [25], [26], [27]]. The pore formation mechanism is associated

with these pyrolysis parameters. Lua and Su [28] revealed that a high pyrolysis temperature, low heating rate, and long soaking times minimized pore formation, which improved its gas selectivity. Salleh and Ismail [29] reported that a higher heating rate produces a more random pore distribution within a CMS material. The pore size and distribution were attributed to an elevated volatile carbon compound removal rate, which may contribute to partial carbon vapor deposition within a formed pore. Meha et al. [30] examined the role of a gas atmosphere's influence on CMS membranes performance. Membranes pyrolyzed in an inert atmosphere versus a vacuum had a more open pore structure and displayed a slightly higher C_2H_4 permeability and lower C_2H_4/C_2H_6 selectivity. The concentration of O_2 during pyrolysis is a critical parameter that controls CMS membrane separation performance. Kiyono et al. [31] investigated the O_2 concentration effects during pyrolysis had a maximum CMS membrane selectivity at 30 ppm was attributed to filling and doping active ultra-micropore sites. These CMS research efforts reveal the importance of O_2 concentration during membrane preparation. The studies suggest that a low pyrolysis temperature, short soaking time, fast heating rate, and an inert pyrolysis atmosphere generally yields a CMS membrane with high gas permeability and low selectivity. Based on these trends, the pyrolysis procedure must be optimized for any given polymer precursor to meet a specific gas separation requirement.

In addition to finely tuning the polymer pyrolysis conditions to create a CMS membrane, precursor modification is an efficient strategy for tailoring its properties. Kim et al. [32] investigated CMS membranes derived from polymers complexed with Li^+, Na^+, and K^+ ions using sulfonated BTDA-BDSA/mPDA polyimides synthesized from benzophenone tetracarboxylic dianhydride (BTDA), 4,4′-diamino 2,2′-biphenyl disulfonic acid (BDSA), and m-phenylenediamine (mPDA). The metal modified CMS membranes' gas permeability increased with alkali metal ion radius attributed to d-spacing variations caused by their size. Yoshimune et al. [33] created metal-containing CMS membranes using sulfonated polyphenylene oxide (SPPO). The technique involved ion-exchanging its –SO_3H groups with monovalent, divalent, and trivalent metal cations (Na^+, Mg^{2+}, Al^{3+}, Ag^+, Cu^{2+}, and Fe^{3+}). CMS membranes derived from SPPO complexed with Ag^+ or Cu^{2+} had significantly improved CO_2 permeability versus CH_4 without affecting its permselectivity. CMS membranes containing Mg^{2+} increased its CO_2 permeability almost four times, but other metal ions such as Na^+, Al^{3+}, and Fe^{3+} only slightly enhanced permselectivity. Chu et al. [34] synthesized a copolymer polyimide using 6FDA, 2,4,6-trimethyl-1,3- phenylenediamine (DAM), and DABA to create a 6FDA-DAM:DABA (3:2). The copolymer's –COOH groups were complexed with Fe^{2+} before pyrolyzing it. The Fe-containing CMS membranes exhibited a 19% increase in C_2H_4/C_2H_6 sorption selectivity (1.2) than a non-Fe containing one. Its selective olefin sorption and affinity improvements were attributed to the Fe complex within the carbon material. Liao et al. [35] created a boron embedded CMS membranes (cPIM) using a hydrolyzed PIM-1 polymer that was complexed with 9,9-dihexylfluorene- 2,7-diboronic acid (DHFDA), which was pyrolyzed at 700 °C. The boron embedded CMS membrane's C_2H_4 permeability was 13.7 Barrer, and its C_2H_4/C_2H_6 selectivity was 9.7, which is a permselectivity enhancement of 82.7% and 4.5%. These previous research efforts reveal that precursor modification is an efficient method needed to improve CMS membrane performance.

In this work, a carboxylated multiblock polyimide with various 6FDA and 4,4'-(hexafluoroisopropylidene) dianiline (6FpDA):DABA molar ratios were synthesized to create

CMS membranes ([Fig. 1](#)). The polyimide's –COOH groups were modified by thermally crosslinking or substituting its proton with a Zn^{2+} ion before pyrolysis. While other research groups have reported using DABA within a precursor polymer to create a CMS, little work has been done tuning the crosslinking degree to tailor its performance. The DABA moieties became crosslinkable sites during decarboxylation or complexation with a divalent ion to create a HOOC-metal-COOH complex. Tuning the 6FpDA:DABA molar ratio optimizes precursor separation performance and membrane microstructure. The DABA concentration within a polyimide affects its intrinsic separation properties, which is one factor impacting a CMS membrane's permselectivity. Metal ion substitution with –COOH groups provides an alternative route that effectively tailors CMS transport properties based upon facilitated transport [36].
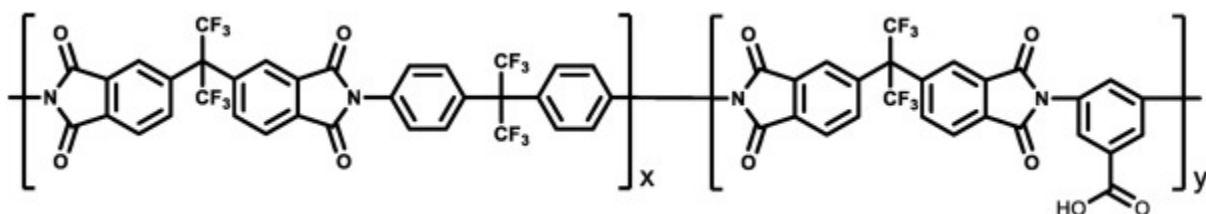
Fig. 1. Chemical structure of 6F-DABA polyimide with *x* and *y* representing 6FDA and DABA molar concentration.

The gas permeation properties of as-prepared 6FDA-6FpDA:DABA polymers, thermally crosslinked ones, and resultant CMS membranes were systematically evaluated using H_2, CO_2, N_2, CH_4, C_2H_4, and C_2H_6. These gases were utilized as molecular probes to detect subtle changes in membrane microstructure. The DABA-free 6FDA-6FpDA membrane's CO_2/CH_4 and C_2H_4/C_2H_6 separation performance was compared to thermally crosslinked 6FDA-6FpDA:DABA, and ones functionalized with Zn^{2+} that were pyrolyzed to create a CMS membrane. All CMS membranes in this work outperformed the precursor membranes, and they had separation properties well beyond the CO_2/CH_4 and C_2H_4/C_2H_6 upper-bound.

2. Experimental section

2.1. Polymer synthesis

A detailed 6FDA-6FpDA polyimide synthesis procedure was reported in previous work [37]. In general, the polyimide was synthesized using stoichiometric amounts of 6FDA and 6FpDA. The monomers were solution polymerized at 190 °C for 12 h and cooled to room temperature after thermal imidization. A controlled amount of 6FDA-6FpDA and 6FDA-DABA were combined and reacted at 190 °C for at least 5 h to generate a multiblock polyimide with various DABA concentrations ranging from 0 to 75%. The following material was precipitated within methanol and dried in a vacuum oven at 100 °C for 24 h to remove residual methanol, water, and solvent. The various polyimides are designated as 6F, 6F-DABA-25, 6F-DABA-50, and 6F-DABA-75. The values 25, 50, and 75 represent the DABA molar percentage (*y*) with the remaining molar amount (*x*) being 6FDA. A representative structure of 6F-DABA with and an arbitrary amount of DABA is shown in [Fig. 1](#). These multiblock polyimides have higher gas separation selectivity than their random copolymer counterpart ([Table S1](#)). A polymer's intrinsic composition,

morphology, and physical properties will significantly affect a CMS membrane's gas separation performance. Therefore, 6F-DABA block copolymers will be studied as CMS membrane precursors rather than random copolymers in this work.

2.2. Membrane preparation

Polymers were dissolved in dimethylacetamide (DMAc) using a concentration of 0.2 g/mL that was stirred for 12 h. Afterward, the solution was allowed to rest at room temperature to remove potential bubbles. The solution was evenly spread on a glass substrate using a doctor blade and dried in an oven at 60 °C for 12 h. A dense polyimide film was produced that was removed from the glass substrate and dried in a vacuum oven at 150 °C for 12 h to remove trace DMAc. The dried polymer film was cut into small circles with a 15 mm die cutter before thermally crosslinking or fabricating into a CMS membrane. The solution-casting process produced films that varied in thickness from 50 to 70 μm.

Metal-ion containing 6F-DABA-50 and 6F-DABA-75 polyimide films were created by immersing in 1 M $ZnNO_3$/MeOH solution at ambient temperature for 24 h. The ion-exchanged film was removed from the $ZnNO_3$/MeOH solution, rinsed to remove excess $ZnNO_3$, and initially dried at ambient conditions. An additional drying step involved using a vacuum oven at 80 °C to remove residual methanol. The resultant membranes were designated as 6F-DABA-50-Zn and 6F-DABA-75-Zn.

2.3. Polymer thermal crosslinking and CMS preparation

Polymer membranes were fixed on a stainless-steel wire support, loaded inside a tubular quartz tube furnace, and thermally treated in it. The furnace was flushed with Argon and then evacuated using a vacuum pump. After repeating this process three times, the furnace was degassed 4 h at ambient conditions. This step was followed by an Argon flush flowing at 400 mL/min to remove residual air from the system. The furnace was continually purged with Argon flowing at 200 mL/min for 2 h before polymer thermal crosslinking and pyrolysis, which keeps the O_2 level below ten ppm confirmed using an oxygen sensor. Polymer thermal crosslinking occurred at 400 °C for 1 h that produced materials denoted as 6F-DABA-Y-C400, where Y is the DABA concentration. All materials were pyrolyzed within an Argon atmosphere following a heating protocol shown in Fig. 2, similar to Qiu and Rungta's work [18,30]. The pyrolysis process was done at three different final temperatures of 576 °C, 700 °C, and 800 °C. The resulting CMS membranes were designated as 6F-DABA-50-CMXX, where XX represents the final pyrolysis temperature. Zn^{2+} functionalized CMS membranes pyrolyzed at 576 °C are called 6F-DABA-Zn576.
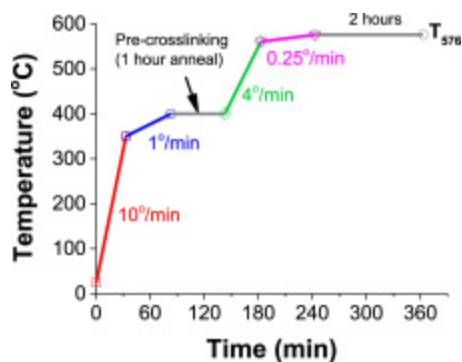
Fig. 2. Pyrolysis heating protocol for a CMS membrane formed at 576 °C.

2.4. Characterization

Thermogravimetric analysis (TGA) and derivative weight data were obtained using a NETZSCH STA 409. An Argon stream was used to create an inert atmosphere, and data were collected from 35 °C to 900 °C at a constant heating rate of 10 °/min. X-ray diffraction (XRD) patterns of the resultant CMS membranes were recorded in a Bruker D8 Advance diffractometer using Cu-Kα radiation (λ = 1.54 Å) at a scanning rate of 4°/min from 5° to 60°. Physisorption data was collected using an ASAP 2020 physisorption analyzer at 273.15 K with CO_2 and an absolute pressure range of 1 to 760 mmHg to characterize its micropore size distribution. The data were analyzed using Quantachrome ASiQwin software and its "CO_2-DFT" model. X-ray photoelectron spectroscopy (XPS) was performed using a Thermo Scientific K-Alpha to measure its elemental composition.

2.5. Gas permeation measurements

All membrane pure and mixed-gas tests were collected using a custom-designed constant-volume/variable-pressure apparatus [38]. Tests were conducted using H_2, N_2, CH_4, CO_2, C_2H_4, and C_2H_6 at a feed pressure of 4 bar and 35 °C. A circular membrane (12 mm) was masked with aluminum tape and epoxy to prevent leakage during all tests. The masked membrane was held in a gas permeation stainless steel flange cell. The upstream and downstream apparatus sections were degassed to a pressure below 0.005 Torr before a test. During the test, pure gases were introduced into the upstream and recorded using a pressure transducer (4 bar), and the permeate cell pressure (downstream) was monitored by an MKS pressure transducer (0–10 Torr). A leak rate test was performed before gas permeation measurements to ensure the gas flux was two orders greater than it, less than 0.00001 Torr/s. Membrane permeability (P) was measured from the gas permeate slope as a function of time, gas diffusivity (D) was calculated from the time-lag technique, and the sorption coefficient (S) was evaluated using the relationship $P = D \times S$. Experimental error is typically not more than 5% for all precursor samples. Overall permeability error is less than 30% for the CMS membranes. The membrane mixed-gas permeation performance was evaluated at 35 °C using a 1:1 M mixture of CO_2:CH_4 and C_2H_4:C_2H_6, similar to previous efforts [[39], [40], [41]]. A mixed-gas test analyzed its downstream composition using a gas chromatograph (Fuli GC9790 Plus).

3. Results and discussion

3.1. Membrane characterization

3.1.1. Thermal analysis of polymer membranes

Precursor membrane TGA and differential TGA curves are shown in Fig. 3. 6F, and 6F-DABA polyimides were thermally stable until 400 °C. They had a mass residue of more than 50 wt% at 900 °C. These results indicate that 6F and 6F-DABA have excellent thermal stability (Fig. 3a). The DABA-free 6F polyimide exhibited a smooth curve near 450 °C. A fast weight loss initiated near 500 °C was caused by backbone degradation with a broad derivative peak at approximately 570 °C.
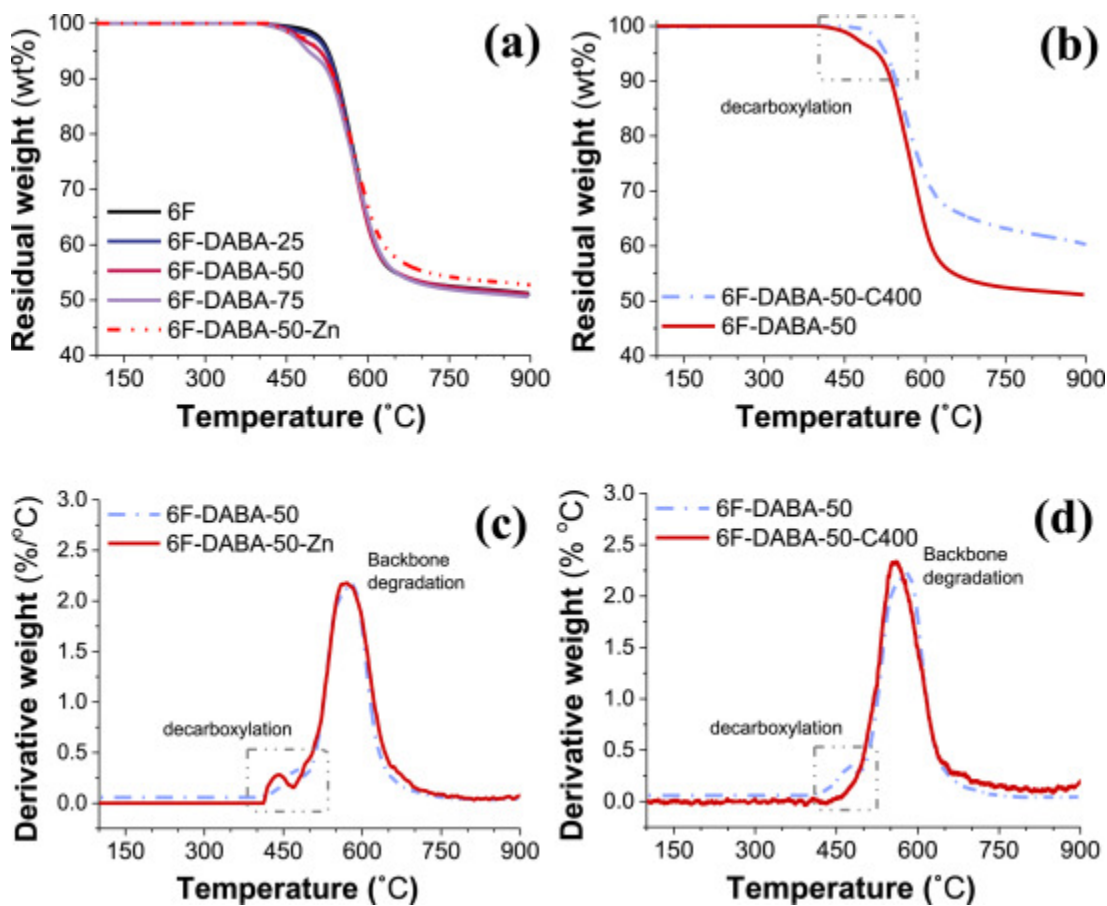
Fig. 3. TGA response for (a) 6F and 6F-DABA, (b) 6F-DABA-50 crosslinked versus non-crosslinked, (c) dynamic TGA response of derivative weight percent for 6F-DABA-50 versus 6F-DABA-50-Zn, and (d) 6F-DABA-50 crosslinked versus non-crosslinked.

DABA introduction into the polymer backbone produced a more substantial weight loss between 400 to 500 °C with a corresponding shoulder peak at 450 °C observed in the derivative weight curve (Fig. 3d). The peak was attributed to DABA decarboxylation that increased with its concentration. The mass loss between 400 to 500 °C followed an order of 6F < 6F-DABA-25 <

6F-DABA-50 < 6F-DABA-75. The mass loss trend is consistent with –COOH concentration within these polyimides. Previous DABA containing polyimide studies have reported thermal crosslinking during –COOH group removal and biphenyl structure formation [15,18,42,43]. As expected, polyimides with a higher 6FpDA:DABA molar ratio produced greater thermal crosslinking reactions.

The as-prepared 6F-DABA-50 thermal stability versus a crosslinked 6F-DABA-50-C400 material is compared in Fig. 3b. The 6F-DABA-50-C400 material had no significant weight loss before 450 °C, which differs from the non-crosslinked one. The thermal decarboxylation thermal event appearing near 450 °C in non-crosslinked samples disappears in 6F-DABA-50-C400 (Fig. 3d). The result suggests that thermal crosslinking and decarboxylation may be complete at 400 °C. As reported in previous studies, thermal annealing at temperatures higher than its T_g can produce a fully crosslinked structure. For example, 6FDA-DAM:DABA (3:2) annealed at 370 °C was completely crosslinked within 1 h [42]. It is expected that 6F-DABA materials are completely crosslinked within 1 h at 400 °C. A solvent test was used to confirm that 6F-DABA-50-C400 was no longer soluble in DMAc due to thermal crosslinking (Fig. S1). The test indicates that crosslinked membranes have excellent chemical resistance.

CMS membrane Zn^{2+} functionalization shows little impact on its thermal stability, as seen in Fig. 3a and c. The Zn^{2+} functionalized 6F-DABA-50-Zn material compared with 6F-DABA-50 reveals an increase in mass residue at 900 °C, which appears to signify its successful incorporation. The existence of a decarboxylation weight loss peak within 6F-DABA-50-Zn indicates that these Zn^{2+} functionalized polymers underwent partial crosslinking at high temperatures.

The 6F-DABA membranes had a maximum degradation rate near 576 °C, as noted from its TGA curve in Fig. 3a. The material's degradation rate slowed down near 700 °C, which was relatively slow beyond 800 °C. Based on its thermal decomposition behavior, final pyrolysis temperatures used to prepare CMS membranes were chosen to be 576 °C, 700 °C, and 800 °C. The pyrolysis temperature of 6F-DABA polyimides was usually higher than its T_g that ranged between 326 °C to 360 °C reported in previous work [44].

3.1.2. XRD

Wide-angle X-ray diffraction patterns of CMS membranes derived from 6F and crosslinked 6F-DABA pyrolyzed at 576 °C are shown in Fig. 4. All samples had a broad amorphous peak at around $2\theta = 24°$, typical of amorphous carbon and its graphitic interplanar space [28]. These material scattering results indicate that CMS membranes were amorphous.
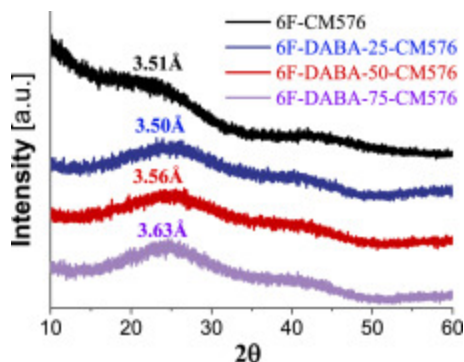
Fig. 4. Wide-angle X-ray diffraction patterns of CMS membranes derived from different polyimide precursors at 576 °C.

The average d-spacing calculated from Bragg's law reflects the interchain distances within an amorphous material. As seen in Fig. 4, a CMS membrane derived from different polyimide precursors had the following average d-spacing order: 6F-DABA-75-CM576 (3.63 Å) > 6F-DABA-50-CM576 (3.56 Å) > 6F-DABA-25-CM576 (3.50 Å) ≅ 6F-CM576 (3.51 Å). As shown in Fig. S2, a Zn^{2+} functionalized CMS membranes' d-spacing did not reveal any consistent trends. The introduction of Zn^{2+} into the polyimide to create 6F-DABA-50-Zn576 led to an increase in d-spacing. A correlation between gas permeability and d-spacing was not obvious that will be discussed later. Consequently, an XRD result is not a holistic tool needed to characterize the ultra-micro structure within a CMS matrix, which has been noted by others [45].

3.1.3. Pore-size distribution of CMS membranes

The pore size distribution of CMS membranes derived from 6F, crosslinked 6F-DABA materials with different DABA moieties, and Zn^{2+} functionalized 6F-DABA-50 materials are shown in Fig. 5. Two peaks are notable at approximately 4.7 Å and 5.5 Å with a similar pore size distribution regardless of CMS membrane precursor type. The almost identical peak location and intensity may suggest that DABA concentration has little influence on pore formation and concentration. Ultra-micropores below 4 Å could efficiently sieve gas molecules, which is expected to exist within a CMS material. Unfortunately, small ultra-micropores with sizes of less than 4 Å cannot be probed using CO_2 sorption isotherm techniques [46].
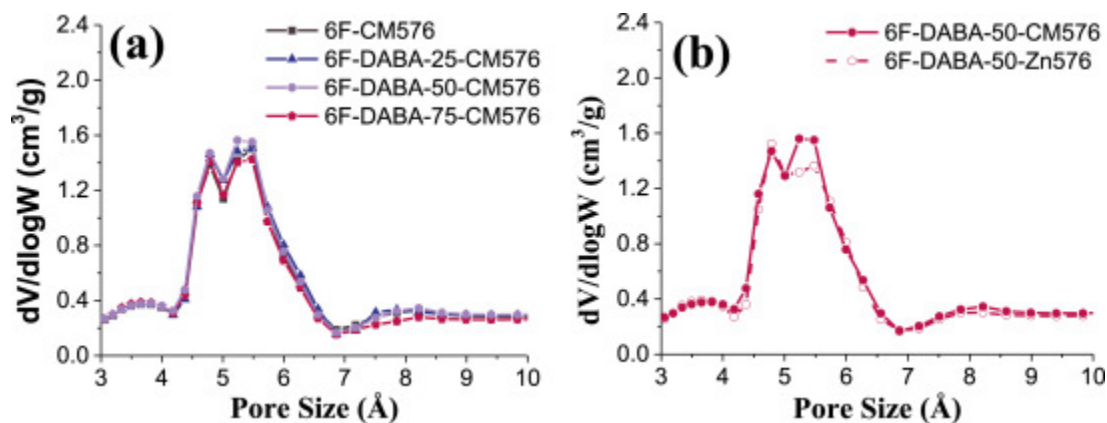
Fig. 5. CMS pore-size distribution created at 576 °C for (a) 6F and 6F-DABA series, and (b) 6F-DABA-50-CM576 versus 6F-DABA-50-Zn576.

6F-DABA-50 derived CMS membranes compared to their Zn^{2+} containing counterparts revealed only subtle pore size distribution differences, which may be within the measurement error (Fig. 5b). These compositional precursors were used to create CMS membranes, and their properties were controlled using DABA concentration and Zn^{2+} complexation. Strictly using pore size and its distribution to identify subtle CMS differences in their structure and ultimate transport properties is challenging. Exclusively using pore size distribution may overlook critical factors that contribute to membrane gas permeability and selectivity. Recent molecular sieving research characterization efforts suggest that gas molecular probes may be the most useful method to study complex CMS materials for gas separation applications [47].

3.1.4. XPS

X-ray photoelectron spectroscopy (XPS) was utilized to investigate the Zn^{2+} metal ion state within 6F-DABA-50-Zn and its carbonized analog. The existence of Zn^{2+} in carbonized materials was confirmed using XPS shown in Fig. 6. The XPS spectra revealed C, N, O, F, and Zn peaks within unpyrolyzed 6F-DABA-50-Zn. The CMS material lacked an F signal, but it possessed distinctive C, N, and O peaks. The result indicates that $-CF_3$ was thermally removed from 6FDA and 6FpDA during pyrolysis. Two binding energy peaks are associated with Zn that are observed at 1020.48 eV (Zn $2p_{3/2}$) and 1043.38 eV (Zn $2p_{1/2}$) shown in Fig. 6b. A constant 22.9 eV binding energy difference between Zn $2p_{3/2}$ and Zn $2p_{1/2}$ is very close to the value of ZnO [48]. The two Zn peaks reveal that Zn^{2+} complexed with carboxylic groups within 6F-DABA-50-Zn are still present within a CMS material (Fig. 6b). The experimental Zn^{2+} concentration within 6F-DABA-50-Zn was approximately 7.61 wt% (theoretical is 8.38 wt%), and its C/Zn ratio was approximately 65. After pyrolysis, the Zn^{2+} concentration decreased to 1.12 wt%, indicating that less Zn^{2+} is present on the membrane's surface. The Zn^{2+} ion loss may be due to surface diffusion to CMS voids that XPS cannot detect. The Zn binding energy changed very little between 6F-DABA-50-Zn and 6F-DABA-50-Zn576, which strongly suggests that the Zn^{2+} chemical state could be unchanged.
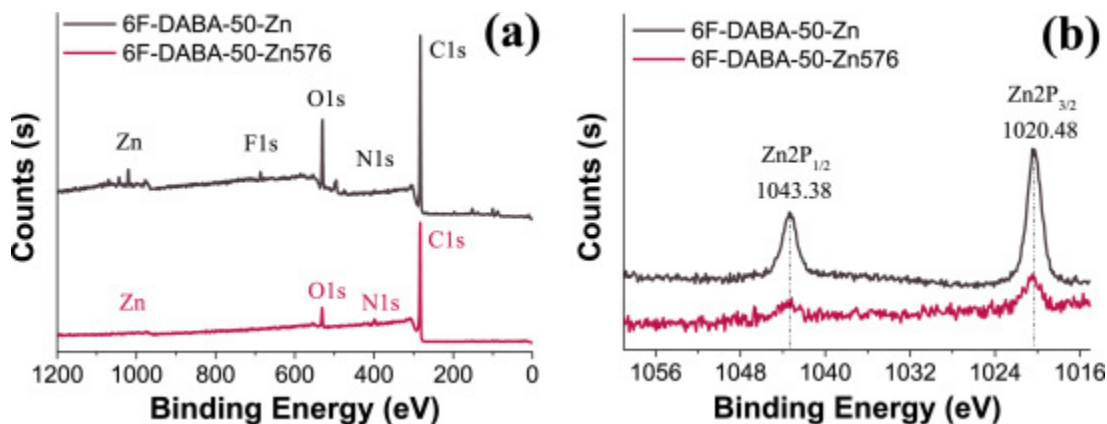
Fig. 6. 6F-DABA-50-Zn and 6F-DABA-50-Zn576 (a) wide scan XPS, and (b) XPS spectra showing Zn $2p_{3/2}$ and Zn $2p_{1/2}$ of materials.

3.2. Gas separation performance

3.2.1. Gas permeation properties of crosslinked 6F-DABA polyimide precursor membranes

All thermally crosslinked 6F-DABA-C400 membranes were created by heating a 6F-DABA film at 400 °C for 1 h. The subsequent membrane's gas permeability was evaluated at 4 bar and 35 °C, summarized in Fig. 7a. The gas permeability of 6F-DABA-C400 increased after being thermally treated at 400 °C, which agrees with previous studies by Qiu et al. using 6FDA-DAM:DABA (3:2) [18,42]. This polymer underwent an unexpected thermal decarboxylation and in-situ crosslinking that produced gas permeability increases for He, O_2, N_2, CH_4, and CO_2 [42]. Similarily, thermally crosslinked 6F-DABA-C400 membranes had better gas separation performance than non-crosslinked ones. 6F-DABA-75-C400 had the largest crosslink density of the 6F-DABA series that is attributed to its DABA group concentration. This elevated crosslinking density led to a more pronounced membrane performance enhancement than non-crosslinked ones. Its H_2/CH_4, CO_2/CH_4, and CO_2/N_2 gas selectivities were 86.8, 42.9, and 21.3, shown in Fig. 7b.
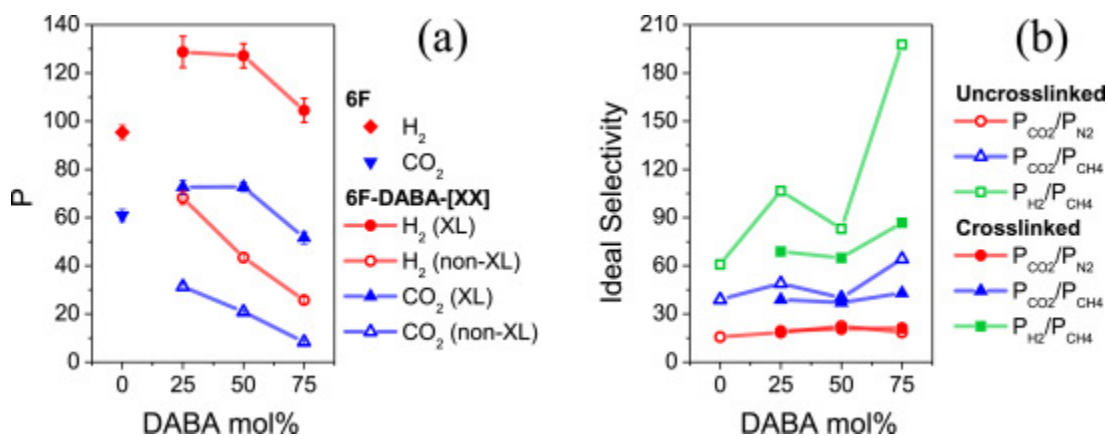
Fig. 7. 6F and 6F-DABA-[XX] crosslinked (XL) and non-crosslinked (non-XL) membrane (a) permeability and (b) ideal selectivity versus DABA mol%. The value [XX] signifies the mole % within the 6F-DABA polyimide.

6F membranes were used as a control to evaluate gas transport performance differences due to DABA. A gas separation performance comparison between 6F and non-crosslinked 6F-DABA (non-XL) reveals lower gas permeability and higher ideal selectivity shown in Fig. 7a and b. Crosslinked (XL) 6F-DABA-C400 membranes' gas permeability and selectivity were more significant than DABA-free 6F material. The gas permeability of 6F-DABA decreased with increasing DABA concentration. In contrast, its concentration has a lower impact on the gas permeability of crosslinked 6F-DABA. For example, the H_2 permeability between crosslinked 6F-DABA-25-C400 and 6F-DABA-50-C400 is nearly identical, but nearly 60% greater than non-XL 6F-DABA-25 and 6F-DABA-50.

In general, thermally crosslinking –COOH groups is used to create the 6F-DABA-C400 series that led to enhancements in gas separation performance. The thermally crosslinked films possessed greater gas permselectivity than its non-XL DABA-free 6F analog. Consequently, 6F-

DABA materials are good precursor candidates for creating CMS membranes. Tuning the DABA molar concentration enables one to optimize its subsequent CMS separation performance.

3.2.2. Pyrolysis temperature effect on CMS membrane performance

6F-DABA-50-C400 films were used to evaluate the role of final pyrolysis temperature on a CMS membrane's separation properties. Many studies examine this relationship, and it is believed that these critical parameters are still required studying to tailor its separation properties [24,45,49]. This relationship was examined using three CMS membranes created from 6F-DABA-50-C400 by pyrolyzing it at 576 °C, 700 °C, and 800 °C. Their carbonized membrane gas separation performance was strongly dependent upon pyrolysis temperature (Fig. 8a). The CMS membrane's gas permeability trend was the following: 6F-DABA-50-CM576 > 6F-DABA-50-CM700 > 6F-DABA-50-CM800. All CMS membrane transport properties outperformed their uncarbonized precursors. For example, 6F-DABA-50-CM576 had H_2, CO_2, and C_2H_4 permeability of 7175, 2609, and 180.6 Barrer. Its CO_2/CH_4, H_2/CH_4, and C_2H_4/C_2H_6 ideal selectivity increased with pyrolysis temperature shown in Fig. 8b. The highest CO_2/CH_4, H_2/CH_4, and C_2H_4/C_2H_6 selectivity were 55.6, 271, and 24.1 obtained with 6F-DABA-50-CM800. The CMS membrane separation performance changes with pyrolysis temperature have been observed by others [28,30]. These transport changes are primarily due to the formation of more compact pores structures with a narrower pore size distribution with increasing pyrolysis temperature [50]. Qiu et al. [18] provided a detailed discussion of these relationships that are described elsewhere.
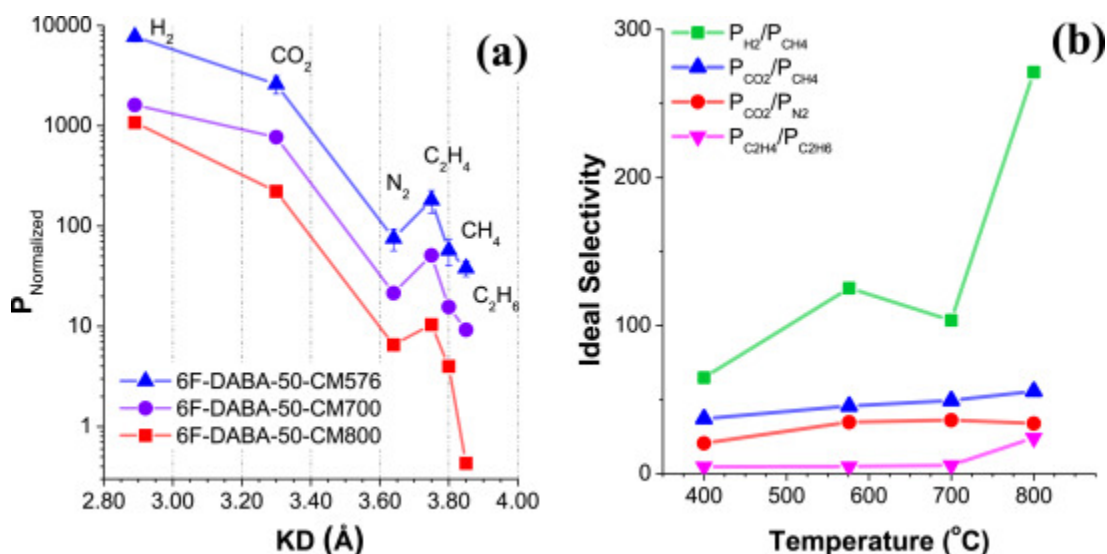
Fig. 8. 6F-DABA-50-CM membrane gas (a) permeability versus KD and (b) ideal selectivity versus pyrolysis temperature.

The 6F-DABA-50 CMS membrane gas permeability and changes with the kinetic diameter (KD) and pyrolysis temperature are shown in Fig. 8 and summarized in Table S3. The following permeability trend was seen: H_2 (2.89 Å) > CO_2 (3.3 Å) > C_2H_4 (3.75 Å) > N_2 (3.64 Å) > CH_4 (3.80 Å) > C_2H_6 (3.85 Å). These permeability results suggest that molecular sieving is the primary transport mechanism in a CMS membrane. Beyond gas size (KD), other critical factors

impacting a membrane's permeation behavior include gas polarity, condensability, shape, and mass. For example, C_2H_4 permeability in the 6F-DABA-50 CMS membrane series is greater than N_2, attributed to its condensability that impacts its solubility [45]. Furthermore, the gas molecule's planar geometry, size, shape, and mass will have a greater impact on its surface diffusion and adsorption than the large condensability of CH_4 [51]. These factors contribute to improved C_2H_4 solubility in these CMS membranes that produces greater permeability than CH_4.

Overall, 6F-DABA-C400 membranes pyrolyzed at increasing temperatures improved its gas selectivity but lowered its permeability. Polymer pyrolysis at 576 °C produced a CMS membrane with the highest gas permeability and lowest selectivity as compared to higher temperatures. The lower-cost 576 °C pyrolysis protocol created CMS materials possessing improved gas permeability well above the upper-bound.

3.2.3. Effect of DABA on CMS membranes separation performance

CMS membranes created at 576 °C had gas permeability and selectivity changes as a function of DABA concentration from 0 to 75% are plotted in Fig. 9. The CMS membrane derived from 6F to create 6F-CM576 had an H_2, CO_2, and C_2H_4 permeability of 3947, 2039, and 166.7 Barrer. The 6F-DABA based CMS membranes had increased gas permeabilities. 6F-DABA-50-CM576 had an H_2, CO_2, and C_2H_4 permeability of 7175, 2609, and 180.6 Barrer. In general, DABA-based CMS membrane's ideal selectivity of H_2/CH_4, CO_2/CH_4, and C_2H_4/C_2H_6 was more significant than a 6F-CMS membrane not having DABA within it (Table S4).
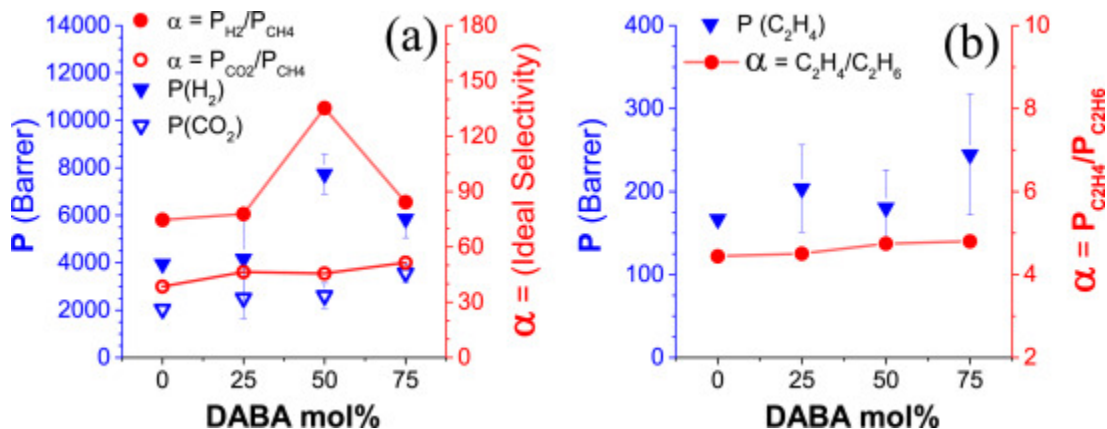
Fig. 9. CMS membranes gas permeability and ideal selectivity trend versus DABA mol% for (a) CO_2/CH_4 and H_2/CH_4, and (b) C_2H_4/C_2H_6.

The enhanced separation properties could be due to crosslinkable precursors not present within a 6F polymer. As previously discussed, crosslinked 6F-DABA gas permeability and selectivity were greater than uncrosslinked 6F (Table S2). Thermal crosslinking of 6F-DABA leads to microvoid formation and polymer chain packing disruptions. Moreover, some polymer chains could be locked in crosslinked polymer chains [42]. These structural effects could be carried forward into the resultant CMS membranes. Therefore, CMS membranes derived from 6F-DABA have improved gas separation performance than DABA-free 6F polyimides.

The 6F-DABA-50-CM576 membrane's H_2/CH_4 selectivity of 135 was the greatest among these four CMS membranes shown in Fig. 9. Its selectivity improvement signifies a greater concentration of ultra-micropores present in the membrane that was not observed within the CO_2 isotherm curves (Fig. 5). Recent CMS pore structural characterization efforts using CO_2 isotherms revealed that it could not detect ultra-micropores that are 4 Å and smaller [45]. Consequently, gas molecular probes may be the most useful method to study complex CMS materials [45,47]. Future efforts beyond this work would involve using advanced characterization methods such as Positron Annihilation Lifetime Spectroscopy to characterize CMS ultra-micropores.

3.2.4. Zn^{2+} functionalization effects on CMS separation performance

6F-DABA-50 and 6F-DABA-75 materials functionalized with Zn^{2+} were pyrolyzed at 576 °C. The subsequent 6F-DABA-50-Zn576 and 6F-DABA-75-Zn576 CMS membrane gas permselectivity performance is summarized in Table 1. The CMS membranes doped with Zn^{2+} led to greater size-selectivity behavior for larger gas molecules than an undoped CMS material. The larger CH_4 and C_2H_6 penetrant molecules compared to H_2 produced a more significant reduction in gas permeability. As a result, H_2 gas selectivity was enhanced over larger gas molecules. For example, 6F-DABA-50-Zn576 and 6F-DABA-75-Zn576 membrane ideal H_2/CH_4 selectivity increased to 170 and 370 from 125 (6F-DABA-50-CM576) and 84.3 (6F-DABA-75-CM576).

Table 1. CMS and Zn^{2+} functionalized CMS membrane gas permeability and ideal selectivity at 35 °C and 4 bar.

Membrane	P (Barrer)					Selectivity		
	H_2	CO_2	C_2H_4	CH_4	C_2H_6	P_{H2}/P_{CH4}	P_{CO2}/P_{CH4}	P_{C2H4}/P_{C2H6}
6F-DABA-50-CM576	7175	2609	180.6	57.29	38.08	125	45.6	4.74
6F-DABA-50-Zn576	7078	2284	137.6	41.49	31.18	170	55.1	4.41
6F-DABA-75-CM576	5852	3573	244.6	69.44	51.01	84.3	51.5	4.80
6F-DABA-75-Zn576	6768	1396	71.16	18.29	10.54	370	76.3	6.75

Generally, divalent metal ions tend to boost gas permeability within facilitated transport membranes by forming π-bonds with CO_2 and C_2H_4 [34]. The H_2 gas molecule is the smallest size with a low critical temperature, condensability, and sorption coefficient within a membrane. A Zn^{2+} functionalized CMS material may have little impact upon its H_2 affinity within it. The observed H_2/CH_4 selectivity changes were mainly attributed to the Zn^{2+} complex occupying and potentially reducing pore channels associated with large molecule transport. The decreased pore sizes and available concentration would impede larger molecules, but smaller molecule diffusion would have a lesser effect. Consequently, the H_2/CH_4 selectivity enhancement is mainly due to a dramatic drop in CH_4 permeability (Table 1).

The CO_2/CH_4 and C_2H_4/C_2H_6 gas pair permeability decreased, and selectivity increased using a Zn^{2+} functionalized 6F-DABA-75-Zn576 membrane. Their reduced permeability was attributed to lower D_{CO2}, and D_{C2H4} noted in Table S5. The membrane's enhanced selectivity was

associated with improved D_{CO2}/D_{CH4}, D_{C2H4}/D_{C2H6}, S_{CO2}/S_{CH4}, and S_{C2H4}/S_{C2H6} properties (Table S6). The 6F-DABA-50-Zn576 and 6F-DABA-75-Zn576 membrane's ideal CO_2/CH_4 selectivity was 55.1 and 76.3, which are 21% and 48% greater than an untreated CMS material.

A 6F-DABA-50-C400 precurosr versus 6F-DABA-50-Zn400 precursor comparison of their ideal CO_2/CH_4 selectivity revealed that Zn^{2+} functionalization improved its permselectivity (Table S2). As discussed earlier, the Zn^{2+} ion improves the membrane's CO_2 affinity due to π-bond formation. Also, its presence may block CO_2 diffusion channels that would lead to improved size exclusion effects. The improved 6F-DABA membrane transport properties created by functionalization with Zn^{2+} may translate into its CMS counterpart, leading to enhanced gas selectivity.

Overall, Zn^{2+} functionalization is an effective method needed to improve CMS membrane gas selectivity. Material performance enhancements are attributed to increased selective adsorption and structural differences caused by the steric effects that improve size-selectivity. Zn^{2+} influenced the CMS membrane's gas affinity due to potential π-bonds forming between an ion and gas. The metal ions' presence changed its microstructure that affects gas diffusivity.

3.2.5. Mixed-gas permeation performance

The relationship between 6F-DABA-50-Zn576 membrane separation performance and operational pressure was explored using an equimolar binary (1:1) mixture of CO_2:CH_4 and C_2H_4:C_2H_6. The CO_2 and C_2H_4 permeability and mixed-gas CO_2/CH_4 and C_2H_4/C_2H_6 selectivity are shown in Table 2. The membrane's CO_2 permeability remained unchanged with feed pressure, but its mixed-gas CO_2/CH_4 selectivity decreased 15.5% from 67.1 to 56.7. The selectivity losses are attributed to competitive sorption effects between CO_2 and CH_4 within the membrane. However, the result is still slightly larger than its ideal selectivity of 55.1. The mixed-gas C_2H_4 permeability increased from 146.6 to 185.4 Barrer created by a feed pressure change from 4 bar to 12 bar, which was accompanied by a C_2H_4/C_2H_6 selectivity decrease. This result suggests that highly absorbing light hydrocarbon gases tend to deteriorate a CMS membranes' gas separation performance at elevated pressure. Notwithstanding, this CMS membrane's mixed-gas separation performance still lies well above the upper-bound (Fig. 10).

Table 2. 6F-DABA-50-Zn576 membrane permeation data using 1:1 M mixtures of CO_2:CH_4 and C_2H_4:C_2H_6 at 35 °C and various pressures.

Pressure (bar)	P (Barrer)		Mixed gas selectivity	
	CO_2	C_2H_4	P_{CO2}/P_{CH4}	P_{C2H4}/P_{C2H6}
4	2566	146.6	67.1	5.52
8	2536	175.7	56.7	4.44
12	–	185.4	–	3.54
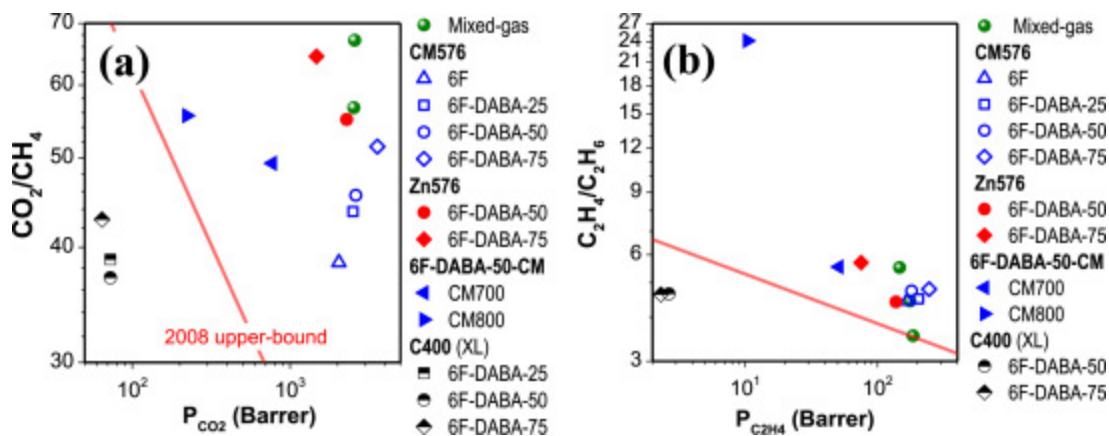
Fig. 10. CMS membrane separation comparison for (a) CO_2/CH_4, and (b) C_2H_4/C_2H_6 gas pairs.

Long-term CMS membrane permeation tests are essential to evaluate their separation performance and stability under operational conditions. They interact with impurities such as water vapor, air, and light hydrocarbons that cause performance losses. The sorption-induced aging phenomena within a CMS membrane has been reported in prior studies [52,53]. However, most losses were reversible using a post-heating treatment or exposure to propylene. Moreover, time-dependent gas separation performance changes are typically associated with high FFV polymers [54]. The physical aging impacts upon CMS membranes warrants additional studies explored in future efforts beyond this work.

3.2.6. Robeson upper-bound comparison

The important CO_2/CH_4 and C_2H_4/C_2H_6 gas pairs were selected to evaluate the CMS membrane's gas separation performance relative to Robeson's upper-bound shown in Fig. 10. The materials surpassed the upper-bound, which is a significant improvement over its unpyrolyzed precursor. The CMS membranes CO_2/CH_4 permselectivity is shown in Fig. 10. It is similar to a CMS membraned derived from 6FDA/DETDA that was pyrolyzed at comparable conditions (Table S7) [14]. The ideal C_2H_4/C_2H_6 selectivity of 6F-DABA-75-Zn576 CMS is 6.75. This result is much higher than a CMS membrane created from PIM-6FDA and 6FDA-DAM:DABA (Table S8) [34,55,56].

Overall, CMS membranes created from 6F-DABA and ones complexed with Zn^{2+} provides excellent gas separation performance. Advancing CMS membrane-based technology requires producing a low-cost material with extensive scalability. A CMS created on a tubular ceramic support offers a scalable route to thin membranes with significantly reduced manufacturing costs. An ultra-thin porous CMS membrane attached to a low-cost porous support could reduce its manufactured cost by 25-fold, as previously discussed by Koros [57]. Assuming the CMS selective layer thickness is three μm on a tubular support, then the CO_2 and C_2H_4 permeability of 6F-DABA-50-Zn576 would be 855 GPU and 48.9 GPU at 35 °C and 4 bar. The CO_2/CH_4 and C_2H_4/C_2H_6 selectivities are 67.1 and 5.52. It is believed that 6F-DABA based CMS membranes have potential industrial application prospects due to their excellent separation performance.

4. Conclusions

6FDA-6FpDA:DABA multiblock polyimides have significant potential for gas separation applications. Their permselectivity properties can be tuned using crosslinking and metal-ion modification. After crosslinking, a 6F-DABA-C400 based membrane displayed improved gas permeability. CMS membranes derived from crosslinked polyimides had a substantial improvement in permeability and selectivity. 6F-DABA-CM576 exhibited improved H_2, CO_2, and C_2H_4 permeability that led to a more considerable ideal selectivity of CO_2/CH_4, H_2/CH_4, and C_2H_4/C_2H_6 as compared to 6F-CM576. The maximum CO_2 and C_2H_4 permeabilities of 3573 Barrer and 244.6 Barrer were achieved using 6F-DABA-75-CM576, which had reasonable CO_2/CH_4 and C_2H_4/C_2H_6 selectivities. The Zn^{2+} functionalized CMS membranes exhibited improved selectivity, which increased from 51.5 to 76.3 for CO_2/CH_4, and 4.80 to 6.75 for C_2H_4/C_2H_6. Mixed-gas tests using 6F-DABA-50-Zn576 revealed higher CO_2/CH_4 and C_2H_4/C_2H_6 selectivities as compared to its ideal selectivity. All the CMS membranes surpassed the upper-bound with an attractive permselectivity performance, especially for ethylene/ethane separation.

CRediT authorship contribution statement

Qixiang Wang: Investigation, Formal analysis, Writing - review & editing. **Fei Huang:** Polymer synthesis. **Chris J. Cornelius:** Conceptualization, Writing - review & editing. **Yanfang Fan:** Conceptualization, Methodology, Supervision, Writing - review & editing.

Declaration of competing interest

The authors declare that they have no known competing financial interests or personal relationships that could have appeared to influence the work reported in this paper.

Acknowledgement

Appendix A. Supplementary data

Solubility tests, detailed CO_2 isotherm, gas permeation data, and comparison of CO_2/N_2, H_2/CH_4 with upper-bound are given in supporting information. These materials are available free of charge via the internet.

The following is the Supplementary data to this article:

Download : Download Word document (274KB)

Multimedia component 1.

Notes

The authors declare no competing financial interest.

References

[1]

W.J. Koros, C. Zhang**Materials for next-generation molecularly selective synthetic membranes**
Nat. Mater., 16 (2017), pp. 289-297
CrossRefView Record in ScopusGoogle Scholar

[2]

O. Sanyal, C. Zhang, G.B. Wenz, S. Fu, N. Bhuwania, L. Xu, M. Rungta, W.J. Koros**Next generation membranes —using tailored carbon**
Carbon, 127 (2018), pp. 688-698
Article
Download PDFView Record in ScopusGoogle Scholar

[3]

K. Maqsood, A. Mullick, A. Ali, K. Kargupta, S. Ganguly**Cryogenic carbon dioxide separation from natural gas: A review based on conventional and novel emerging technologies**
Rev. Chem. Eng., 30 (2014)
Google Scholar

[4]

J. Kim, D.A. Pham, Y.I. Lim**Gas-liquid multiphase computational fluid dynamics (CFD) of amine absorption column with structured-packing for CO_2 capture**
Comput. Chem. Eng., 88 (2016), pp. 64-66
CrossRefView Record in ScopusGoogle Scholar

[5]

A. Jomekian, B. Bazooyar, R.M. Behbahani, T. Mohammadi, A. Kargari**Ionic liquid-modified Pebax® 1657 membrane filled by ZIF-8 particles for separation of CO_2 from CH_4, N_2 and H_2**
J. Membr. Sci., 524 (2016), pp. 652-662
Google Scholar

[6]

I. Erucar, S. Keskin**Computational assessment of MOF membranes for CH_4/H_2 separations**
J. Membr. Sci., 514 (2016), pp. 313-321
Article
Download PDFView Record in ScopusGoogle Scholar

[7]

A. Kargari, A. Arabi Shamsabadi, M. Bahrami Babaheidari**Influence of coating conditions on the H$_2$ separation performance from H$_2$/CH$_4$ gas mixtures by the PDMS/PEI composite membrane**
Int. J. Hydrogen Energy, 39 (2014), pp. 6588-6597
Article
Download PDFView Record in ScopusGoogle Scholar

[8]

O.M. Ilinich, K.I. Zamaraev**Separation of ethylene and ethane over polyphenyleneoxides membranes: Transient increase of selectivity**
J. Membr. Sci., 82 (1993), pp. 149-155
Article
Download PDFView Record in ScopusGoogle Scholar

[9]

Y. Zheng, N. Hu, H. Wang, N. Bu, F. Zhang, R. Zhou**Preparation of steam-stable high-silica CHA (SSZ-13) membranes for CO$_2$/CH$_4$ and C$_2$H$_4$/C$_2$H$_6$ separation**
J. Membr. Sci., 475 (2015), pp. 303-310
Article
Download PDFView Record in ScopusGoogle Scholar

[10]

L.M. Robeson**Correlation of separation factor versus permeability for polymeric membranes**
J. Membr. Sci., 62 (1991), pp. 165-185
Article
Download PDFView Record in ScopusGoogle Scholar

[11]

L.M. Robeson**The upper bound revisited**
J. Membr. Sci., 320 (2008), pp. 390-400
Article
Download PDFView Record in ScopusGoogle Scholar

[12]

J. Koresh, A. Soffer**A molecular sieve carbon membrane for continuous process gas separation**
Carbon, 22 (1984)
225-220
Google Scholar

[13]

S. Fu, E.S. Sanders, S.S. Kulkarni, W.J. Koros**Carbon molecular sieve membrane structure-property relationships for four novel 6FDA based polyimide precursors**
J. Membr. Sci., 487 (2015), pp. 60-73
Article
Download PDFView Record in ScopusGoogle Scholar

[14]

S. Fu, E.S. Sanders, S.S. Kulkarni, G.B. Wenz, W.J. Koros**Temperature dependence of gas transport and sorption in carbon molecular sieve membranes derived from four 6FDA based polyimides: Entropic selectivity evaluation**
Carbon, 95 (2015), pp. 995-1006

Article

Download PDFView Record in ScopusGoogle Scholar

[15]

S. Fu, G.B. Wenz, E.S. Sanders, S.S. Kulkarni, W. Qiu, C. Ma, W.J. Koros**Effects of pyrolysis conditions on gas separation properties of 6FDA/DETDA:DABA(3:2) derived carbon molecular sieve membranes**
J. Membr. Sci., 520 (2016), pp. 699-711
Article

Download PDFView Record in ScopusGoogle Scholar

[16]

G.B. Wenz, W.J. Koros**Tuning carbon molecular sieves for natural gas separations: A diamine molecular approach**
AIChE J., 63 (2017), pp. 751-760
CrossRefView Record in ScopusGoogle Scholar

[17]

C. Zhang, R. Kumar, W.J. Koros**Ultra-thin skin carbon hollow fiber membranes for sustainable molecular separations**
AIChE J., 65 (2019)
Google Scholar

[18]

W. Qiu, K. Zhang, F.S. Li, K. Zhang, W.J. Koros**Gas separation performance of carbon molecular sieve membranes based on 6FDA-mPDA/DABA (3:2) polyimide**
ChemSusChem, 7 (2014), pp. 1186-1194
CrossRefView Record in ScopusGoogle Scholar

[19]

S. Fu, E.S. Sanders, S. Kulkarni, Y.-H. Chu, G.B. Wenz, W.J. Koros**The significance of entropic selectivity in carbon molecular sieve membranes derived from 6FDA/DETDA:DABA(3:2) polyimide**
J. Membr. Sci., 539 (2017), pp. 329-343
Article

Download PDFView Record in ScopusGoogle Scholar

[20]

C. Karunaweera, I.H. Musselman, K.J. Balkus, J.P. Ferraris**Fabrication and characterization of aging resistant carbon molecular sieve membranes for C_3 separation using high molecular weight crosslinkable polyimide, 6FDA-DABA**
J. Membr. Sci., 581 (2019), pp. 430-438
Article

Download PDFView Record in ScopusGoogle Scholar

[21]

Y.K. Kim, H.B. Park, Y.M. Lee**Preparation and characterization of carbon molecular sieve membranes derived from BTDA–ODA polyimide and their gas separation properties**
J. Membr. Sci., 255 (2005), pp. 265-273
Article

Download PDFView Record in ScopusGoogle Scholar

[22]

J.I. Hayashi, H. Mizuta, M. Yamamoto, K. Kusakabe, S. Morooka**Pore size control of carbonized BPDA-pp'ODA polyimide membrane by chemical vapor deposition of carbon**
J. Membr. Sci., 124 (1997), pp. 243-251
Article
Download PDFView Record in ScopusGoogle Scholar

[23]

K.M. Steel, W.J. Koros**An investigation of the effects of pyrolysis parameters on gas separation properties of carbon materials**
Carbon, 43 (2005), pp. 1843-1856
Article
Download PDFView Record in ScopusGoogle Scholar

[24]

P.S. Tin, T.-S. Chung, Y. Liu, R. Wang**Separation of CO2/CH4 through carbon molecular sieve membranes derived from P84 polyimide**
Carbon, 42 (2004), pp. 3123-3131
Article
Download PDFView Record in ScopusGoogle Scholar

[25]

V.C. Geiszler, W.J. Koros**Effects of polyimide pyrolysis conditions on carbon molecular sieve membrane properties**
Ind. Eng. Chem. Res., 35 (1996), pp. 2999-3003
View Record in ScopusGoogle Scholar

[26]

Y. Zhou, Y. Wang, Y. Ban, A. Guo, K. Yang, N. Cao, W. Yang**Carbon molecular sieving membranes for butane isomer separation**
AIChE J. (2019), p. 65
Article
Download PDFView Record in ScopusGoogle Scholar

[27]

H. Suda, K. Haraya**Gas permeation through micropores of carbon molecular sieve membranes derived from kapton polyimide**
J. Phys. Chem. B, 101 (1997), pp. 3988-3994
View Record in ScopusGoogle Scholar

[28]

A.C. Lua, J. Su**Effects of carbonisation on pore evolution and gas permeation properties of carbon membranes from Kapton® polyimide**
Carbon, 44 (2006), pp. 2964-2972
Article
Download PDFView Record in ScopusGoogle Scholar

[29]

W.N.W. Salleh, A.F. Ismail**Effects of carbonization heating rate on CO_2 separation of derived carbon membranes**
Separ. Purif. Technol., 88 (2012), pp. 174-183
Article
Download PDFView Record in ScopusGoogle Scholar

[30]

M. Rungta, L. Xu, W.J. Koros**Carbon molecular sieve dense film membranes derived from Matrimid® for ethylene/ethane separation**
Carbon, 50 (2012), pp. 1488-1502
Article
Download PDFView Record in ScopusGoogle Scholar

[31]

M. Kiyono, P.J. Williams, W.J. Koros**Effect of pyrolysis atmosphere on separation performance of carbon molecular sieve membranes**
J. Membr. Sci., 359 (2010), pp. 2-10
Article
Download PDFView Record in ScopusGoogle Scholar

[32]

Y. Kim**Carbon molecular sieve membranes derived from metal-substituted sulfonated polyimide and their gas separation properties**
J. Membr. Sci., 226 (2003), pp. 145-158
Article
Download PDFView Record in ScopusGoogle Scholar

[33]

M. Yoshimune, I. Fujiwara, H. Suda, K. Haraya**Gas transport properties of carbon molecular sieve membranes derived from metal containing sulfonated poly(phenylene oxide)**
Desalination, 193 (2006), pp. 66-72
Article
Download PDFView Record in ScopusGoogle Scholar

[34]

Y.-H. Chu, D. Yancey, L. Xu, M. Martinez, M. Brayden, W. Koros**Iron-containing carbon molecular sieve membranes for advanced olefin/paraffin separations**
J. Membr. Sci., 548 (2018), pp. 609-620
Article
Download PDFView Record in ScopusGoogle Scholar

[35]

K.-S. Liao, S. Japip, J.-Y. Lai, T.-S. Chung**Boron-embedded hydrolyzed PIM-1 carbon membranes for synergistic ethylene/ethane purification**
J. Membr. Sci., 534 (2017), pp. 92-99
Article
Download PDFView Record in ScopusGoogle Scholar

[36]

Y. Li, S. Wang, G. He, H. Wu, F. Pan, Z. Jiang**Facilitated transport of small molecules and ions for energy-efficient membranes**
Chem. Soc. Rev., 44 (2015), pp. 103-118
CrossRefView Record in ScopusGoogle Scholar

[37]

F. Huang, C.J. Cornelius**Polyimide-SiO2-TiO2 nanocomposite structural study probing free volume, physical properties, and gas transport**
J. Membr. Sci., 542 (2017), pp. 110-122

Article

Download PDFView Record in ScopusGoogle Scholar

[38]

J. Comyn**Introduction to polymer permeability and the mathematics of diffusion**
Polymer Permeability (1985), pp. 1-10
CrossRefView Record in ScopusGoogle Scholar

[39]

K.C. O'Brien, W.J. Koros, T.A. Barbari, E.S. Sanders**A new technique for the measurement of multicomponent gas transport through polymeric films**
J. Membr. Sci., 29 (1986), pp. 229-238
Article

Download PDFView Record in ScopusGoogle Scholar

[40]

Y. Fan, C. Li, X. Zhang, X. Yang, X. Su, H. Ye, N. Li**Tröger 's base mixed matrix membranes for gas separation incorporating NH2-MIL-53(Al) nanocrystals**
J. Membr. Sci., 573 (2019), pp. 359-369
Article

Download PDFCrossRefView Record in ScopusGoogle Scholar

[41]

Y. Fan, H. Yu, S. Xu, Q. Shen, H. Ye, N. Li**Zn(II)-modified imidazole containing polyimide/ZIF-8 mixed matrix membranes for gas separations**
J. Membr. Sci., 597 (2020), p. 117775
Article

Download PDFGoogle Scholar

[42]

W. Qiu, C.-C. Chen, L. Xu, L. Cui, D.R. Paul, W.J. Koros**Sub-tg cross-linking of a polyimide membrane for enhanced CO2 plasticization resistance for natural gas separation**
Macromolecules, 44 (2011), pp. 6046-6056
CrossRefView Record in ScopusGoogle Scholar

[43]

M. Askari, T.-S. Chung**Natural gas purification and olefin/paraffin separation using thermal cross-linkable co-polyimide/ZIF-8 mixed matrix membranes**
J. Membr. Sci., 444 (2013), pp. 173-183
Article

Download PDFView Record in ScopusGoogle Scholar

[44]

F. Huang, A. Tahmasbi Rad, W. Zheng, M.P. Nieh, C.J. Cornelius**Hybrid organic-inorganic 6FDA-6pFDA and multiblock 6FDA-DABA polyimide SiO₂–TiO₂ nanocomposites: synthesis, FFV, FTIR, swelling, stability, and X-ray scattering**
Polymer, 108 (2017), pp. 105-120
Article

Download PDFView Record in ScopusGoogle Scholar

[45]

M. Rungta, L. Xu, W.J. Koros**Structure–performance characterization for carbon molecular sieve membranes using molecular scale gas probes**

Carbon, 85 (2015), pp. 429-442

[Article](#)

[Download PDFView Record in ScopusGoogle Scholar](#)

[46]

M. Rungta, G.B. Wenz, C. Zhang, L. Xu, W. Qiu, J.S. Adams, W.J. Koros**Carbon molecular sieve structure development and membrane performance relationships**
Carbon, 115 (2017), pp. 237-248

[Article](#)

[Download PDFView Record in ScopusGoogle Scholar](#)

[47]

J.S. Adams, A.K. Itta, C. Zhang, G.B. Wenz, O. Sanyal, W.J. Koros**New insights into structural evolution in carbon molecular sieve membranes during pyrolysis**
Carbon, 141 (2019), pp. 238-246

[Article](#)

[Download PDFView Record in ScopusGoogle Scholar](#)

[48]

D. Sahu, N.R. Panda, B.S. Acharya, A.K. Panda**Microstructural and optical investigations on sonochemically synthesized Cu doped ZnO nanobricks**
Ceram. Int., 40 (2014), pp. 11041-11049

[Article](#)

[Download PDFView Record in ScopusGoogle Scholar](#)

[49]

Z. Wang, H. Ren, S. Zhang, F. Zhang, J. Jin**Carbon molecular sieve membranes derived from troger's base-based microporous polyimide for gas separation**
ChemSusChem, 11 (2018), pp. 916-923

[Article](#)

[Download PDFView Record in ScopusGoogle Scholar](#)

[50]

S.S. Hosseini, M.R. Omidkhah, A. Zarringhalam Moghaddam, V. Pirouzfar, W.B. Krantz, N.R. Tan**Enhancing the properties and gas separation performance of PBI–polyimides blend carbon molecular sieve membranes via optimization of the pyrolysis process**
Separ. Purif. Technol., 122 (2014), pp. 278-289

[Article](#)

[Download PDFView Record in ScopusGoogle Scholar](#)

[51]

M. Rungta, Z. Chen, W.J. Koros, L. Xu**Membrane-based ethylene/ethane separation: the upper bound and beyond**
AIChE J., 59 (2013), pp. 3475-3489

[CrossRefView Record in ScopusGoogle Scholar](#)

[52]

S. Lagorsse, F.D. Magalhães, A. Mendes**Aging study of carbon molecular sieve membranes**
J. Membr. Sci., 310 (2008), pp. 494-502

[Article](#)

[Download PDFView Record in ScopusGoogle Scholar](#)

[53]

I. Menendez, A.B. Fuertes**Aging of carbon membranes under different environments**
Carbon, 39 (2001), pp. 733-740
Article
Download PDFView Record in ScopusGoogle Scholar

[54]

L. Xu, M. Rungta, J. Hessler, W. Qiu, M. Brayden, M. Martinez, G. Barbay, W.J. Koros**Physical aging in carbon molecular sieve membranes**
Carbon, 80 (2014), pp. 155-166
Article
Download PDFView Record in ScopusGoogle Scholar

[55]

O. Salinas, X. Ma, E. Litwiller, I. Pinnau**High-performance carbon molecular sieve membranes for ethylene/ethane separation derived from an intrinsically microporous polyimide**
J. Membr. Sci., 500 (2016), pp. 115-123
Article
Download PDFView Record in ScopusGoogle Scholar

[56]

O. Salinas, X. Ma, Y. Wang, Y. Han, I. Pinnau**Carbon molecular sieve membrane from a microporous spirobisindane-based polyimide precursor with enhanced ethylene/ethane mixed-gas selectivity**
RSC Adv., 7 (2017), pp. 3265-3272
CrossRefView Record in ScopusGoogle Scholar

[57]

Y. Cao, K. Zhang, O. Sanyal, W.J. Koros**Carbon molecular sieve membrane preparation by economical coating and pyrolysis of porous polymer hollow fibers**
Angew. Chem. Int. Ed., 58 (2019), pp. 12149-12153
CrossRefView Record in ScopusGoogle Scholar
View Abstract